

Measurement of ^{15}N relaxation rates in perdeuterated proteins by TROSY-based methods

Nils-Alexander Lakomek · Jinfa Ying ·
Ad Bax

Received: 4 March 2012 / Accepted: 4 April 2012 / Published online: 12 June 2012
© Springer Science+Business Media B.V. (outside the USA) 2012

Abstract While extracting dynamics parameters from backbone ^{15}N relaxation measurements in proteins has become routine over the past two decades, it is increasingly recognized that accurate quantitative analysis can remain limited by the potential presence of systematic errors associated with the measurement of ^{15}N R_1 and R_2 or $R_{1\rho}$ relaxation rates as well as heteronuclear ^{15}N - $\{^1\text{H}\}$ NOE values. We show that systematic errors in such measurements can be far larger than the statistical error derived from either the observed signal-to-noise ratio, or from the reproducibility of the measurement. Unless special precautions are taken, the problem of systematic errors is shown to be particularly acute in perdeuterated systems, and even more so when TROSY instead of HSQC elements are used to read out the ^{15}N magnetization through the NMR-sensitive ^1H nucleus. A discussion of the most common sources of systematic errors is presented, as well as TROSY-based pulse schemes that appear free of systematic errors to the level of $<1\%$. Application to the small perdeuterated protein GB3, which yields exceptionally high S/N and therefore is an ideal test molecule for detection of systematic errors, yields relaxation rates that show considerably less residue by residue variation than previous measurements. Measured R_2'/R_1' ratios fit an axially symmetric diffusion tensor with a Pearson's

correlation coefficient of 0.97, comparable to fits obtained for backbone amide RDCs to the Saupe matrix.

Keywords Backbone dynamics · Relaxation · TROSY · Perdeuterated proteins · Cross-correlated relaxation · Water saturation

Introduction

It is well recognized that quantitative knowledge of the amplitudes and time scales of internal motions in proteins presents a key complement to the time-averaged coordinates of the structure, determined by X-ray crystallography or NMR spectroscopy. NMR relaxation measurements are the most widely used and versatile experimental methods to gain access to this dynamic information (Kay 1998; Ishima and Torchia 2000; Kern and Zuiderweg 2003; Palmer 2004; Mittermaier and Kay 2006; Cavanagh et al. 2007). They can yield semi-quantitative insights into the hard to grasp entropic component of the free energy of a protein and its change upon ligand or target binding (Yang et al. 1997; Zidek et al. 1999; Lee et al. 2000; Lee and Wand 2001; Li and Brueschweiler 2009), the role of dynamics in enabling allosteric transitions (Kern and Zuiderweg 2003; Popovych et al. 2006; Namanja et al. 2011), distinction between induced fit versus conformational selection binding modes (Hare et al. 1999; Stone 2001; Varadan et al. 2004; Mittag et al. 2010; Rinnenthal et al. 2011), as well as provide a baseline to evaluate the trajectories generated by the wide range of molecular dynamics programs and force fields (Stocker and van Gunsteren 2000; Price and Brooks 2002; Hornak et al. 2006; Showalter and Bruschweiler 2007). Sensitive, ^1H -detected NMR relaxation measurements include a wide

Electronic supplementary material The online version of this article (doi:10.1007/s10858-012-9626-5) contains supplementary material, which is available to authorized users.

N.-A. Lakomek · J. Ying · A. Bax (✉)
Laboratory of Chemical Physics (LCP), DHHS NIDDK,
National Institutes of Health, Building 5, Room 126,
9000 Rockville Pike, Bethesda, MD 20892-0520, USA
e-mail: bax@nih.gov

range of experimental approaches, including the classic backbone ^{15}N relaxation measurements (Kay et al. 1989; Peng et al. 1991), ^{13}C relaxation measurements (Sklenar et al. 1987; Nirmala and Wagner 1988), measurements of dipolar cross-correlated relaxation rates (Tjandra et al. 1996; Felli et al. 1998; Yang et al. 1998; Pelupessy et al. 1999), ^2H relaxation rates in deuterated systems (Muhandiram et al. 1995; Millet et al. 2002), as well as a host of ingenious multi-quantum and other relaxation measurements (Reif et al. 1997; Chiarparin et al. 1999).

Of the various types of relaxation measurements, backbone ^{15}N experiments are generally the most sensitive and also the most widely used. However, it is becoming increasingly recognized that even though the high sensitivity makes such measurements very precise, and frequently highly reproducible, systematic errors in such measurements can be substantially larger than random errors. Systematic errors prove to be particularly problematic for measurements in perdeuterated systems, where TROSY-readout elements (Pervushin et al. 1997, 1998; Nietlispach 2005) are needed to gain adequate spectral resolution. For example, without special precautions, ^{15}N - $\{^1\text{H}\}$ NOE values greater than 1, or even >1.5 , could be measured, far above the theoretical limit of about 0.8 (Zhu et al. 2000; Chill et al. 2006). Indeed, as we will demonstrate here, the use of TROSY readout elements can exacerbate the impact of cross-correlated relaxation effects on measured rates. Use of perdeuteration, frequently needed when using TROSY detection schemes, also makes the results increasingly sensitive to the handling of the water magnetization during the pulse scheme, which can have a rather severe impact on measured apparent ^{15}N R_1 and $R_{1\rho}$ or R_2 rates (Chen and Tjandra 2011). Although the need to fully saturate the water signal in such experiments, or to completely eliminate any saturation of the water signal, was realized early on (Farrow et al. 1994), introduction of cryogenic probeheads can complicate manipulation of the water signal and numerous subsequent modifications of the relaxation experiments no longer strictly adhere to these early recommendations.

In this study we evaluate a number of problems that exist in commonly used pulse schemes (Kay et al. 1989; Zhu et al. 2000; Chill et al. 2006) which can lead to systematic errors in the measured ^{15}N relaxation rates. We describe and discuss a set of experiments with TROSY detection modules, which have been optimized for highly deuterated systems, but which are equally applicable to smaller protonated samples. Although the TROSY-detected relaxation measurements are of primary benefit for large systems, where the TROSY line narrowing is most important, we evaluate the performance of the experiments on the small, perdeuterated third Igg-binding domain of protein G (GB3), because it yields exceptionally high

signal to noise and thereby allows detection of even very small systematic errors. We demonstrate that the experiments yield accurate ^{15}N R_1 and $R_{1\rho}$ relaxation rates, as reflected in exceptionally tight fits between observed R_2'/R_1' ratios and values predicted for an axially symmetric diffusion tensor. ^{15}N - $\{^1\text{H}\}$ NOE values measured with the new scheme are remarkably uniform and, except for two loop regions and the terminal residues, fall close to values predicted for a rigid rotor, i.e. indicative of very limited spectral density near the ^1H Larmor frequency. Application of the experiments to slower tumbling, larger systems requires adjustment of the variable ^{15}N relaxation and interscan delays to account for the faster transverse and slower longitudinal relaxation rates, but does not introduce new problems.

Experimental section

NMR spectroscopy

Data were recorded on a 1.3 mM uniformly ^{15}N , ^2H -enriched sample of GB3, dissolved in 25 mM NaH_2PO_4 buffer (pH 6.4), 0.01 % NaN_3 , and 5 % D_2O . The protein was expressed and purified as described previously (Nadaud et al. 2007).

TROSY-based R_1 , $R_{1\rho}$ and ^{15}N - $\{^1\text{H}\}$ NOE experiments were carried out with a variety of pulse schemes, as described in the Results and Discussion section, but final optimal performance was obtained with the pulse schemes shown in Fig. 1, and the corresponding HSQC-detected analogous experiments presented in Supplementary Material (SM) Fig. S1. Spectra were recorded at 298 K on a 600 MHz Bruker Advance II, equipped with a TCI cryogenic probehead and a z-gradient accessory. The spectral dimensions were 2,000 Hz (F_1) and 8,417 Hz (F_2), corresponding to 32.9×14 ppm, with sampling durations of 30 ms (t_1) and 122 ms (t_2). For each relaxation time measurement, the relaxation decay was sampled for 8 different delay durations, and the FIDs recorded for these delay durations were recorded prior to incrementation of the t_1 evolution period. For each value of t_1 , the order of the relaxation delay durations was pseudo-randomized (R_1 delays: 0, 240, 400, 80, 320, 160, 480 and 560 ms; $R_{1\rho}$ delays: 20, 210, 1, 160, 100, 190, 50, 290 ms). The strength of the radiofrequency (RF) spin-lock field during $R_{1\rho}$ measurement ($\nu_{\text{RF}} = 1.4$ kHz) was limited by the long spin lock durations (up to 290 ms) needed to sample sufficient ^{15}N magnetization decay for the small, slowly relaxing GB3 protein. RF carriers were at 4.75 ppm for ^1H , at 119 ppm for ^{15}N , and at 176 ppm for ^{13}C . Eight scans per FID were recorded for all TROSY-based experiments and four scans for the HSQC-detected experiments, with a

Fig. 1 Pulse schemes for measurement of ^{15}N relaxation rates through TROSY ^1H detection in perdeuterated, amide-protonated proteins. **a** Scheme for measurement of ^{15}N R_1 . Substitution of the element shown in **b** for the *red-bracketed* element in **a** converts the experiment to a ^{15}N $R_{1\rho}$ measurement. **c** Pulse scheme for measurement of ^{15}N - $\{^1\text{H}\}$ NOE. *Narrow* and *wide pulses* correspond to 90° and 180° flip angle pulses, respectively, with phase x unless otherwise indicated. The rectangular low amplitude ^1H pulses marked $-x$ and $x + \phi$ are low power 90° pulses (1.2 ms at 600 MHz); shaped low power ^1H pulses (1.9 ms) correspond to the center lobe of a $(\sin x)/x$ function, all serving to return the water magnetization to z prior to detection (Pervushin et al. 1998). For application to samples that also are enriched in ^{13}C : durations of ^{13}C pulses (all 180°) are equal to $\frac{\sqrt{\Omega}}{2\pi}$ (47.4 μs at 600 MHz), where Ω is the frequency difference between $^{13}\text{C}^\alpha$ and $^{13}\text{C}'$. Delay durations are $\delta = 2.65$ ms and ε corresponds to the duration of the decoding gradient G_4 (60.8 μs ; the slight offset ($\varepsilon/2$) relative to the ^{15}N 180° pulse enables insertion of the decoding gradient G_4 , without introducing a linear phase error in the ^1H dimension). Gradients: G_0 (2.65 ms; 2.1 G/cm), G_1 (2.65 ms; 1.4 G/cm), G_2 (300 μs ; 7 G/cm), G_3 (1 ms; 35 G/cm) and G_9 (T/4; 0.35 G/cm) are rectangular shaped. Gradients G_5 (300 μs ; -23 G/cm), G_4 (60.8 μs ; 23 G/cm), G_6 (1 ms; 19.6 G/cm), G_7 (200 μs ; -35 G/cm) and G_8 (200 μs , 28 G/cm) are sine-bell shaped. Phase cycling $\phi_6 = 4(y), 4(-y)$; $\phi_7 = y, x, -y, -x$; $\phi_1 = y$; $\phi_{\text{rec}} = y, -x, -y, x, -y, x, y, -x$. Quadrature detection is implemented using the Rance-Kay echo/anti-echo scheme (Kay et al. 1992) with the polarity of gradients G_5 and $-G_5$ inverted, and phase $\phi_7 = y, -x, -y, x$ and $\phi_1 = -y$ for the second FID generated for each quadrature pair. **a** The 180° ^1H pulse applied at the midpoint of T (40 ms) is of the IBURP2 type and has a 2 ms duration (at 600 MHz). The loop is repeated an even number of times ($n = 0, 2, \dots$). ^{13}C 180° pulses serve to eliminate cross correlation effects resulting from ^{15}N - ^{13}C dipolar interaction in samples that include ^{13}C labeling. To ensure that the same RF heating applies in the R_1 and $R_{1\rho}$ experiments, immediately following data acquisition, a ^{15}N temperature compensation pulse (Wang and Bax 1993) is applied that corresponds to the longest spin-lock time and RF power of the $R_{1\rho}$ experiment (see below). The 90° ^{15}N pulse (*red*) preceding this temperature compensation pulse eliminates $^{15}\text{N}_z$ magnetization, transferred from ^1H to ^{15}N by the TROSY readout scheme (Favier and Brutscher 2011). **b** The triangle shaped RF fields preceding and following the spin-lock

period are adiabatic half passage (AHP) pulses (Mulder et al. 1998) and correspond to the first and second half (3 ms each) of a tangent hyperbolic tangent (\tanh/\tan) adiabatic inversion pulse as defined in the Bruker shaped pulse library (100 kHz total sweep width, $\zeta = 10$, and $\tan(\kappa) = 20$) with a maximum RF field strength $\omega_{1,\text{max}}$ identical to that used for the spin lock period. The amplitude modulation of the AHP \tanh/\tan pulse is $\omega_1(t) = \omega_{1,\text{max}} \tanh(\zeta t/\tau)$ and the frequency offset $\Delta\omega(t) = \Delta\omega_{\text{max}} \tan[\kappa(1 - t/\tau)]/\tan(\kappa)$, with τ being the duration of the first adiabatic half passage pulse (3 ms) (Garwood and Ke 1991; Mulder et al. 1998). The minimum required duration τ of the AHP pulse scales inversely with the strength of the spin lock field. To eliminate the effect of cross-correlated relaxation, composite $90_x-210_y-90_x$ ^1H pulses (compensated for RF-inhomogeneity and offset) are applied at T/4 and 3T/4. H_2O radiation damping between the two composite pulses is prevented by the very weak (0.35 G/cm) gradient G_9 which is inverted at the midpoint. For ^{13}C -enriched samples, 180° $^{13}\text{C}^\alpha$ and $^{13}\text{C}'$ pulses are applied to cancel possible cross-correlated relaxation effects related to the ^{15}N - ^{13}C dipolar coupling. A temperature compensation RF field (50 kHz off-resonance) is applied at the strength used during T, for a duration that equals the difference of the current and the maximum spin-lock duration, and is part of the magnetization recovery delay between scans, t_{recov} , which is independent of the duration of T. **c** ^1H saturation is achieved by n repetitions of the symmetric ($\Delta-180^\circ-\Delta$) unit (Ferrage et al. 2010), with the ^1H carrier switched to 8.6 ppm and Δ equal to 11 ms ($\approx 1/J_{\text{NH}}$). After saturation, the ^1H carrier is switched back to the H_2O resonance. During the ^{15}N coherence encoding, a composite $90_x-210_y-90_x$ proton pulse (*red*) is applied to interchange the TROSY and anti-TROSY components, such that the scheme actually measures the magnetization of the anti-TROSY component just prior to the 90_{ϕ_7} ^{15}N pulse. Effective rotation of the water magnetization by the composite pulse is about an axis that deviates from the y axis, and the low power $^1\text{H}_2\text{O}$ pulse following the composite pulse requires a correction phase $\phi \approx (210^\circ-180^\circ)$, empirically optimized for minimal H_2O excitation, yielding $\phi = 27^\circ$ on our system. The first 90° ^{15}N pulse (*red*) is applied immediately after data acquisition and serves to eliminate $^{15}\text{N}_z$ magnetization, transferred from ^1H by the TROSY readout element. The delay τ equals the time needed for half the ^1H WATERGATE element plus the encoding gradient G_5 and the gradient recovery delay

recovery delay between scans of 3.5 s unless noted otherwise. With the ^1H T_1 varying between 1 and 4 s for different GB3 residues, a recovery delay of 3.5 s was chosen as a compromise. With these parameters, the total experimental time was ca. 8 h for the TROSY-based measurements and ca. 4 h for the HSQC-based measurements. The impact of using a much shorter, 1-s recovery delay was also evaluated, and found to be negligible (SM Fig. S5).

The ^{15}N - $\{^1\text{H}\}$ NOE and reference spectra were recorded in an inter-leaved manner, with either a 10 s or 5 s ^1H saturation time for the NOE experiment and the equivalent recovery time for the reference experiment, each preceded by an additional 1 s recovery time. Spectral settings were identical to those for the R_1 and $R_{1\rho}$ measurements; but 4 scans were recorded per FID, resulting in total experimental time of ca. 6 h (10 s ^1H saturation) or 3 h (5 s ^1H saturation). Spectra were processed and analyzed using the NMRPipe software package (Delaglio et al. 1995). Spectral

intensities and relaxation rates were extracted with NMRPipe scripts which, together with Bruker pulse sequence code, can be downloaded from <http://spin.niddk.nih.gov/bax/pp/>. R_2 rates were corrected for the off-resonance tilted field, using the relation

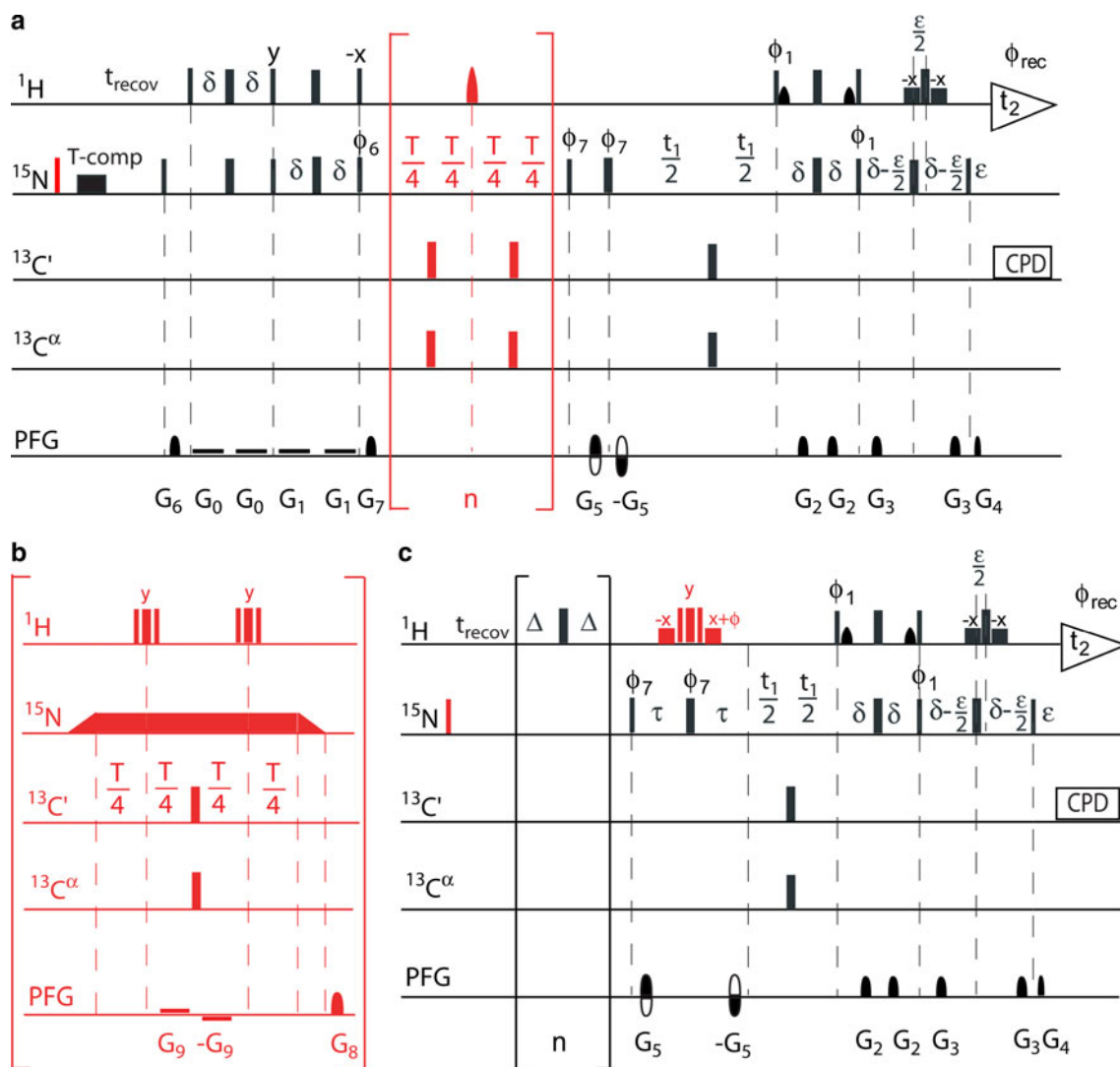
$$R_2 = R_{1\rho} / \sin^2 \theta - R_1 / \tan^2 \theta \quad (1)$$

with $\tan \theta = \omega_1/\Omega$, where ω_1 is the spin-lock RF field strength and Ω the offset from the ^{15}N carrier.

The data were compared to measurements that used a variety of other widely used pulse schemes, including different methods for the removal of cross-correlated relaxation during the variable R_1 and $R_{1\rho}$ relaxation delay.

Diffusion tensor calculation

To assess the quality of the data, an axially symmetric diffusion tensor (Tjandra et al. 1995; Fushman et al. 1999;



Hall and Fushman 2003; Walker et al. 2004) was fitted to the measured relaxation rates using the program ROTDIF (Walker et al. 2004).

Results and discussion

As was highlighted very recently in an independent study by Chen and Tjandra (Chen and Tjandra 2011), measurements of ^{15}N relaxation rates can be quite sensitive to details of the water magnetization trajectory during the course of the pulse sequence. Partial saturation of water magnetization during the pulse sequence, together with its relatively slow longitudinal relaxation rate (ca 0.3 s^{-1}), can significantly attenuate the amide proton signal intensities. This attenuation takes place primarily through ^1H – ^1H NOE to nearby exchangeable protons or through direct hydrogen exchange with the water magnetization. Efforts are

sometimes made to avoid such attenuation by using water-flip-back elements in the pulse sequence or pulses with zero excitation at the water-resonance (Grzesiek and Bax 1993; Farrow et al. 1994; Zhu et al. 2000; Chill et al. 2006). If not done, a variable degree of water saturation will often occur with the change in the ^{15}N relaxation delay, unless explicit water presaturation is used in the delay between scans or other schemes are used to saturate the water magnetization. In particular, in R_1 and $R_{1\rho}$ measurements a variable number of non-selective 180° ^1H pulses is commonly used to eliminate the effect of relaxation interference between ^{15}N – ^1H dipolar and ^{15}N CSA relaxation mechanisms (Boyd et al. 1990; Peng and Wagner 1992; Farrow et al. 1994). Progressive attenuation of water magnetization associated with an increasing number of 180° ^1H pulses for longer values of the ^{15}N relaxation decay period will decrease the amount of amide ^1H magnetization available at the start of the next transient, unless

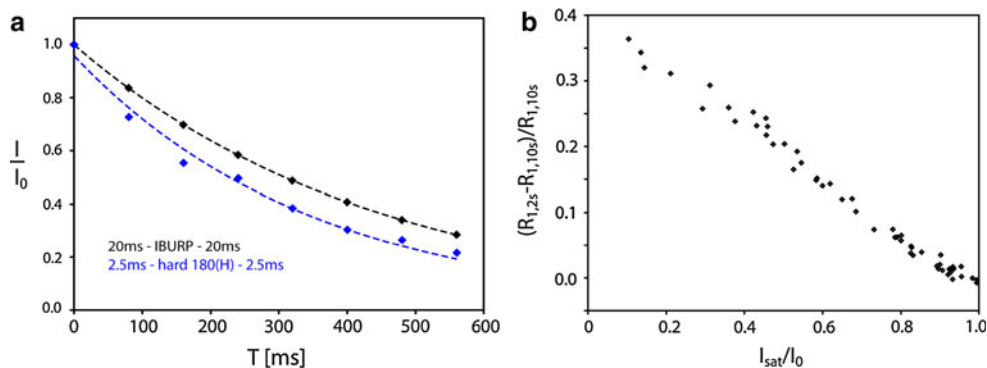


Fig. 2 Impact of progressive water saturation during the ^{15}N relaxation delay on the apparent R_1 ^{15}N decay rate. **a** Comparison of the intensity decay profile of the ^1H - ^{15}N correlation of Thr 17 when measured with the pulse scheme of Fig. 1a, using H^{N} -selective IBURP pulses (*black symbols*) with 40 ms separation and non-selective ^1H pulses (*blue*) with 5 ms separation to remove dipole-CSA cross correlation. The intensity of the first data point ($T = 0$) has been normalized to 1, and therefore superimposes for the two data sets. *Dashed lines* correspond to the least squares exponential fits. **b** Comparison of the fractional increase in the R_1 relaxation rates,

$(R_{1,2s} - R_{1,10s})/R_{1,10s}$, with the degree of saturation I_{sat}/I_0 observed when preceding a water-flip-back HSQC experiment by water pre-saturation. $R_{1,2s}$ and $R_{1,10s}$ are the R_1 rates with 2 and 10 s duration between scans, in both cases using non-selective 180° pulses with 5 ms separation to remove cross correlation. When using a 10 s interscan delay, the effect of water saturation by these 180° pulses has dissipated when the next scan is started, and $R_{1,10s}$ values correspond closely to the true R_1 values measured when using IBURP 180° pulses (Fig. 1a) and a 3.5 s interscan delay (compare also SM Fig. S2b)

a delay time between scans much greater than the water T_1 is used, or an explicit effort is made to saturate the water signal (Peng and Wagner 1992). Less available H^{N} magnetization at the start of the pulse sequence for longer ^{15}N relaxation decay periods (compared to shorter relaxation decay durations, when fewer 180° ^1H pulses are applied and less water saturation has occurred) manifests itself as a faster decay of the HSQC or TROSY intensities, when plotted as a function of the ^{15}N decay duration (Fig. 2a), i.e. as a systematic increase in the apparent relaxation rate. Indeed, the fractional increase in the apparent R_1 rate when using non-selective ^1H 180° pulses to remove cross correlation, separated by 5 ms, instead of H^{N} -selective IBURP pulses, separated by 40 ms, closely correlates with the intensity loss observed in an HSQC spectrum when the water signal is presaturated, versus when it is not (Fig. 2b).

The effect of increased levels of water saturation with longer ^{15}N relaxation delays applies equally to HSQC- and TROSY-detected versions of the experiments. However, for perdeuterated proteins, where the TROSY-based experiments are most profitable, the impact of water saturation on the amide H^{N} magnetization often is much more severe than for fully protonated proteins. The reason for this is that as a result of the diluted ^1H spin density in a perdeuterated, amide-protonated protein, the amide proton has fewer cross relaxation pathways to return to thermal equilibrium at the end of each transient, while being subjected to approximately the same rate of attenuation caused by direct and indirect magnetization exchange with the partially saturated water as in protonated proteins. Indeed, a substantial fraction of the amide protons are attenuated by

50 % or more when the water signal is presaturated (Fig. 2b).

The procedures described below, which aim to eliminate the variable degree of water saturation, are equally applicable to HSQC- and TROSY-detected versions of the experiments. However, the use of TROSY detection is found to additionally require particular care in ensuring complete elimination of antiphase magnetization at the start of the ^{15}N relaxation decay period. In contrast to HSQC-detected experiments, where such an antiphase component to first order does not contribute to observed magnetization, TROSY-detected experiments convert the $\text{N}^{\text{H}}\beta$ magnetization, present during t_1 evolution, into observed $^1\text{H}^{\text{N}}$ signal. This happens regardless of whether the $\text{N}^{\text{H}}\beta$ TROSY component existed as in-phase ^{15}N , or as antiphase magnetization during the ^{15}N relaxation decay period. However, the decay rate of antiphase magnetization is impacted by the finite lifetime of the H^{N} spin state, and therefore will be faster than that of in-phase magnetization. Depending on the sign of residual N_zH_z relative to that of the in-phase N_z term, just prior to the variable ^{15}N relaxation delay, the observed rate may be higher or lower than the true rate. For this reason it is important to eliminate possible small antiphase terms in TROSY-detected experiments. The pulse schemes optimized for ^{15}N relaxation measurements in perdeuterated proteins are depicted in Fig. 1, and will be shown to yield rates that are virtually indistinguishable from similarly optimized experiments that utilize a gradient-enhanced HSQC element to convert ^{15}N magnetization back to ^1H for detection (SM Fig. S1).

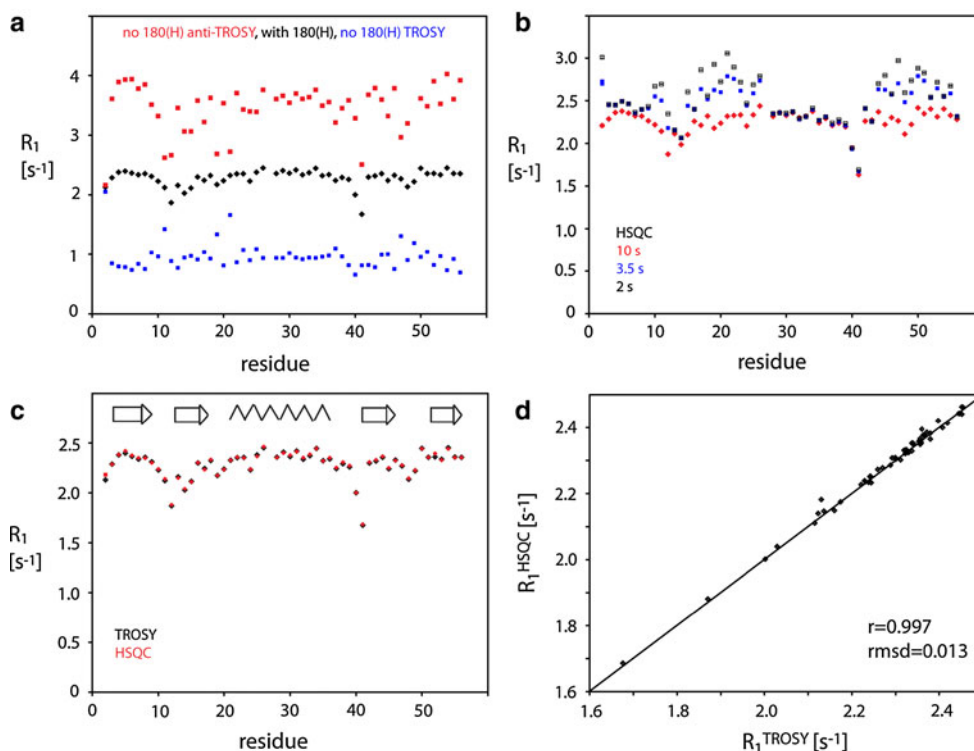


Fig. 3 R_1 relaxation rates measured for perdeuterated GB3. **a** R_1 relaxation rates measured when no 180° (^1H) pulses are applied during the T_1 delay and either TROSY (blue) or anti-TROSY (red) readout is used, and R_1 rates with cross-correlated relaxation removed (black) using the pulse scheme of Fig. 1a. **b** R_1 relaxation rates measured using hard 180° ^1H pulses, separated by a 5-ms delay, for suppressing cross-correlated relaxation. The apparent rates measured with a recovery delay of 2 s (black) and 3.5 s (blue) are increased

Accurate measurement of the $^{15}\text{N}\{-^1\text{H}\}$ NOE in perdeuterated proteins by TROSY-detection also requires particular care compared to HSQC-detected schemes. Details will be discussed below in the description of the pulse scheme.

Measurement of R_1

The impact of relaxation interference between $^{15}\text{N}\{-^1\text{H}\}$ dipolar and ^{15}N CSA relaxation mechanisms on the decay rate of ^{15}N magnetization has long been recognized and causes the down-field component of the $^{15}\text{N}\{-^1\text{H}\}$ doublet to relax much more slowly than the upfield component (Fig. 3a). Although cross-correlated relaxation forms the basis for the TROSY experiment (Pervushin et al. 1997), and clearly can be highly beneficial in protein NMR, its presence complicates interpretation of relaxation rates. Fortunately, its effect in ^{15}N relaxation measurements can be readily eliminated by decoupling the ^1H spins during the variable ^{15}N magnetization decay period, T , either by means of composite pulse decoupling or by application of 180° ^1H pulses (Boyd et al. 1990). Although, in principle,

compared to 10 s (red), both for HSQC detection (data shown) as well as TROSY detection (data not shown). **c** Comparison of R_1 relaxation rates measured with the TROSY read out (black) and measured with sensitivity-enhanced HSQC readout (red) (see Fig. S1a). **d** Correlation plot of R_1 relaxation rates measured with TROSY and sensitivity-enhanced HSQC read out. Random errors fall within the size of the symbols in all four panels

application of a single 180° applied at the midpoint of T would suffice for this purpose, the finite lifetime for the spin state of the ^{15}N -attached ^1H makes it necessary to apply multiple 180° pulses, at a rate that is much faster than the inverse of the $^1\text{H}^{\text{N}}$ spin lifetime (Cavanagh et al. 2007). Application of multiple 180° ^1H pulses also mitigates the effect of incomplete spin inversion associated with non-ideality of these inversion pulses, which are invariably impacted by resonance offset and RF inhomogeneity.

Below we compare measurements carried out with several variations on the optimized TROSY-detected pulse scheme of Fig. 1a. When the 180° ^1H pulses are not applied during the ^{15}N T_1 relaxation delay, T , the very slow relaxation rate of the downfield, TROSY-component of the $^{15}\text{N}\{-^1\text{H}\}$ doublet component is measured (Fig. 3a, blue), whereas approximately fourfold faster R_1 values are obtained when relaxation of the upfield, anti-TROSY component is measured (Fig. 3a, red). When 180° ^1H IBURP pulses are applied during the T -period (Fig. 1a), the average of the two rates is observed (Fig. 3a, black). Note that for protonated proteins the apparent difference between the R_1 relaxation rates of the upfield and

downfield ^{15}N - $\{^1\text{H}\}$ doublet component tends to be considerably smaller than shown here for perdeuterated GB3 because ^1H spin flips, resulting from effective ^1H - ^1H cross relaxation, induce exchange between the longitudinal $\text{N}\{-\text{H}^{\text{N},\alpha}\}$ and $\text{N}\{-\text{H}^{\text{N},\beta}\}$ doublet components at a rate that is comparable to or faster than their R_1 difference. Analogously, for amide protons that rapidly exchange with solvent, e.g. Q2, K10, T11 and G41 in GB3, the apparent difference in relaxation rates between the two doublet components is much smaller than for more slowly exchanging amide protons. In perdeuterated proteins, the spin state lifetime of slowly or non-exchanging H^{N} nuclei is considerably longer than in protonated proteins, and it is therefore important that equal amounts of the two doublet components are present at the start of the T period. For this purpose, a 90°_{-x} purge pulse is applied just prior to T (Fig. 1a), such as to eliminate any antiphase N_zH_z terms. This purge pulse simultaneously serves the purpose of returning the water magnetization back to the $+z$ axis. Measurements carried out with HSQC detection schemes simply observe the sum of both ^{15}N doublet components and to first order are not affected by the residual presence of a small antiphase component at the start of T. As discussed above, it is important that water magnetization is not attenuated during the ^{15}N relaxation delay T, in particular for amide sites whose ^1H magnetization exchanges with that of water. For this purpose, we use H^{N} -selective IBURP pulses (Geen and Freeman 1991), which do not affect the water magnetization. Alternatively, a WATER-GATE-like combination (Piotto et al. 1992) of selective and non-selective pulses (Chen and Tjandra 2011) (SM Fig. S3a) or a cosine modulated 180° (^1H) pulse with zero excitation at the water resonance can be used for this purpose (Farrow et al. 1994). However, when applying such pulses it is important to ensure that no significant saturation of the $^1\text{H}_2\text{O}$ magnetization occurs during the pulses themselves, or from the cumulative effect of imperfection in such pulses. Thus, pulses need to be applied fast enough to eliminate the effect of cross-correlated relaxation, but at the same time attenuation of the water magnetization must remain minimal. We find that a 40-ms delay between 180° pulses is sufficiently short relative to the inverse of the CSA-dipolar longitudinal cross-correlated relaxation rate ($\leq \sim 2 \text{ s}^{-1}$ for GB3, Fig. 3a, and smaller for larger proteins) (SM Fig. S2a). However, a systematic increase in ^{15}N R_1 rates is observed for amides whose magnetization is most impacted by saturation of the H_2O resonance (Fig. 3b) if ^{15}N R_1 measurements are carried out using non-selective 180° pulses with a 5-ms spacing (SM Fig. S3b), widely used in the literature, and no explicit saturation of the water magnetization is used. Note that saturation of the water signal can dramatically decrease the signal to noise ratios for amides that are in

exchange with water, or that are in close proximity to amide or hydroxyl protons that exchange with water, and is therefore undesirable.

As mentioned above, the impact of partial saturation of water magnetization during T applies to both HSQC- and TROSY-detected versions of the experiment. The progressive decrease in signal intensity with increased saturation of H_2O as a function of T sometimes can be difficult to distinguish from the natural decay resulting from ^{15}N R_1 relaxation. Comparison of the rates measured with non-selective and H^{N} -selective IBURP pulses shows a systematic overestimate when non-selective ^1H 180° pulses are used to remove cross correlation. The fractional overestimate of the R_1 rate correlates closely with the level of attenuation, I_{sat}/I_0 , observed in HSQC spectra recorded with and without presaturation of the H_2O resonance (Fig. 2b). However, as expected, the magnitude of the overestimate decreases when the delay between scans is increased (Fig. 3b; SM Fig. S2b). Indeed, for a long recycle delay of 10 s R_1 rates measured using non-selective ^1H 180° pulses agree well with those measured using H^{N} -selective IBURP pulses. The good agreement also shows that 40-ms spacing between IBURP pulses is sufficient to remove the effects of cross-correlated relaxation in GB3. For larger proteins with slower rotational diffusion, both ^{15}N R_1 and ^1H R_1 rates will decrease, and the same applies for the longitudinal CSA-dipolar cross-correlated relaxation rate. Therefore, for large proteins, the 40-ms spacing remains sufficiently short to effectively remove the effect of CSA-dipolar cross-correlated relaxation.

When comparing the R_1 relaxation rates measured for GB3 with TROSY-detection (Fig. 1a) and those obtained with HSQC-detection (Fig. S1a), no systematic differences are seen and a very small root mean square difference (rmsd) in the rates (0.013 s^{-1} , or ca 0.5 %) is obtained, with values being highly uniform in regions of regular secondary structure (Fig. 3c, d).

Measurement of $R_{1\rho}$

For the $R_{1\rho}$ measurement, where the total ^{15}N relaxation delay never extends much beyond the lifetime of the amide ^1H spin, application of two 180° ^1H pulses suffices to remove the effects of cross-correlated relaxation. The two 180° ^1H are positioned at T/4 and 3T/4 (Fig. 1b) and as discussed below, it is important that they be close to ideal in their ability to invert the ^1H spin state. The advantages of using a limited number of 180° ^1H pulses over alternative decoupling schemes, such as WALTZ or application of 180° ^1H pulse trains, similar to what is used for T_1 measurements, have been pointed out previously (Korzhnev et al. 2002). In this respect, the use of only two pulses has been identified as the method of choice (Massi et al. 2004). Note

that for larger molecules the rate of transverse CSA-dipolar cross-correlated relaxation increases—but so does the R_2 auto-relaxation rate. Therefore, much shorter spin lock durations are required to sample the exponential decay curve, thereby reducing the maximum spacing between the two 180° ^1H composite pulses.

Remarkably, in contrast to HSQC-detected experiments, TROSY-detected experiments require the use of an even number of symmetrically placed pulses during the spin lock period to eliminate the net effect of ^1H spin flips during the spin lock period. When only a single 180° ^1H pulse is applied (Chill et al. 2006) at the center of the spin lock delay, T , the net effect of ^1H spin flips will result in incomplete cancellation of cross-correlation and lead to a reduced apparent $R_{1\rho}$ rate (Fig. 4b) (for a detailed explanation, see SM and Fig. S4). For HSQC-detected experiments, this second-order cross correlation effect does not significantly impact the observed signal as the increase in TROSY component to first order is canceled by a decrease in the anti-TROSY component, and it is the sum of the two that defines the observed ^1H HSQC intensity.

As is the case with the R_1 measurements, it is important to ensure that the water resonance is minimally saturated, and that the trajectory of the water magnetization is as similar as possible between different durations of the spin lock duration, T . In principle, this could be accomplished by surrounding the 180° ^1H pulses by water-flip back pulses (Chen and Tjandra 2011), or by using band-selective ^1H pulses. However, the finite duration of such pulses forces the shortest T duration to be rather long, a potential problem in the application to larger proteins where TROSY-detection is most needed. As only two 180° pulses are used to remove the effect of cross correlated relaxation, making the effect of any imperfection far more severe than for the case where a series of such pulses is used (as applies for the R_1 measurement), the ^1H 180° pulses are of the offset- and RF inhomogeneity-compensated type, $90_x-210_y-90_x$ (Freeman et al. 1980). This short composite pulse is fully adequate for our purposes. Alternatively, even better but slightly longer inversion pulses such as BIP (Smith et al. 2001) or BIBOP (Kobzar et al. 2008) may be used, but require a slightly longer minimal duration of the

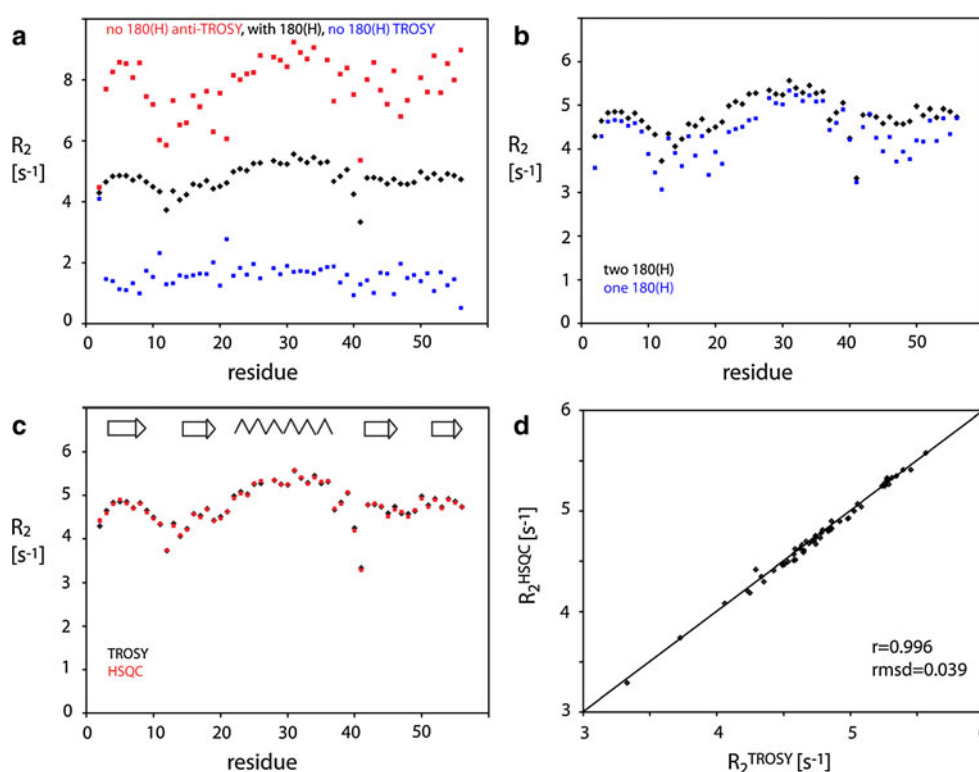


Fig. 4 R_2 relaxation measurements with TROSY detection. $R_{1\rho}$ values were measured with the scheme of Fig. 1b, and R_2 rates were extracted using Eq. 1. **a** R_2 relaxation rates measured when no $180^\circ(^1\text{H})$ pulses are applied during the delay, T , and either TROSY (blue) or anti-TROSY (red) magnetization is read, as well as the rates when the effect of cross-correlated relaxation is eliminated using the pulse sequence of Fig. 1b (black). **b** R_2 relaxation rates measured with

a single 180° (^1H) proton pulse (plus one water flip-back pulse) (blue), applied at the mid-point of T , systematically underestimate the true R_2 rates (black). **c** Comparison of R_2 relaxation rates measured with the TROSY readout (black) and measured with sensitivity-enhanced HSQC readout (red) (see Fig. S1b). **d** Correlation plot of R_2 relaxation rates measured with TROSY readout and sensitivity-enhanced HSQC readout

spin lock period, T . In order to avoid the water magnetization from returning to $+z$ after the first of these two pulses through the radiation damping mechanism, a very weak field gradient is applied (0.35 G/cm). Although some water T_1 relaxation will occur before the second ^1H 180° pulse is applied, a time $T/2$ later, this attenuation is negligible for most practical purposes as $T/2 \ll T_1^{\text{H}_2\text{O}}$. A potential drawback of the applied weak field gradient during the spin-lock period is that it changes the offset of the spin-locked ^{15}N magnetization, by an amount that depends on the position in the sample. For this reason it is important that the gradient is kept very weak, but strong enough to prevent water radiation damping. On our instrument, a 0.35 G/cm suffices for this purpose, introducing offsets not exceeding ± 90 Hz for spins within ± 6 mm from the gradient coil center. In the absence of water-flip-back pulses or a gradient between the two 180° ^1H pulses, radiation damping will occur relatively rapidly, and the second 180° ^1H pulse can rotate the water magnetization to a poorly defined state, resulting in water suppression problems during the detection stage for certain durations of T , in addition to the variable degree of water saturation encountered for different T duration.

A well-known problem in $R_{1\rho}$ measurement is to obtain precise alignment of the ^{15}N magnetization with the spin lock field, regardless of the offset of any given spin. If magnetization is not perfectly aligned, the component orthogonal to the spin lock field will decay relatively rapidly and can give rise to small, offset-dependent phase distortions in the final spectrum, which become smaller with increasing values of T . A variety of solutions to achieve optimal alignment by means of RF pulses have been devised over the years (Bothnerby and Shukla 1988; Hansen and Kay 2007), or alternatively an adiabatic half passage pulse can be used for this purpose (Mitschang et al. 1992). However, in our hands we find it difficult to prevent the phase distortions to the desired level, below 1°, in particular for the shortest T values. Instead, we therefore opt to encapsulate the spin lock period by z filters (Mulder et al. 1998) (Fig. 1b), and thereby ensure all spectra to have identical phasing for all durations of T .

With a pairwise rmsd of $0.039 \text{ s}^{-1} \text{ Hz}$, and a Pearson's correlation coefficient of 0.996, R_2 rates derived from our $R_{1\rho}$ measurement using Eq. 1. agree to better than 1 % with those measured with the analogous HSQC-detected experiment (Fig. 4c, d).

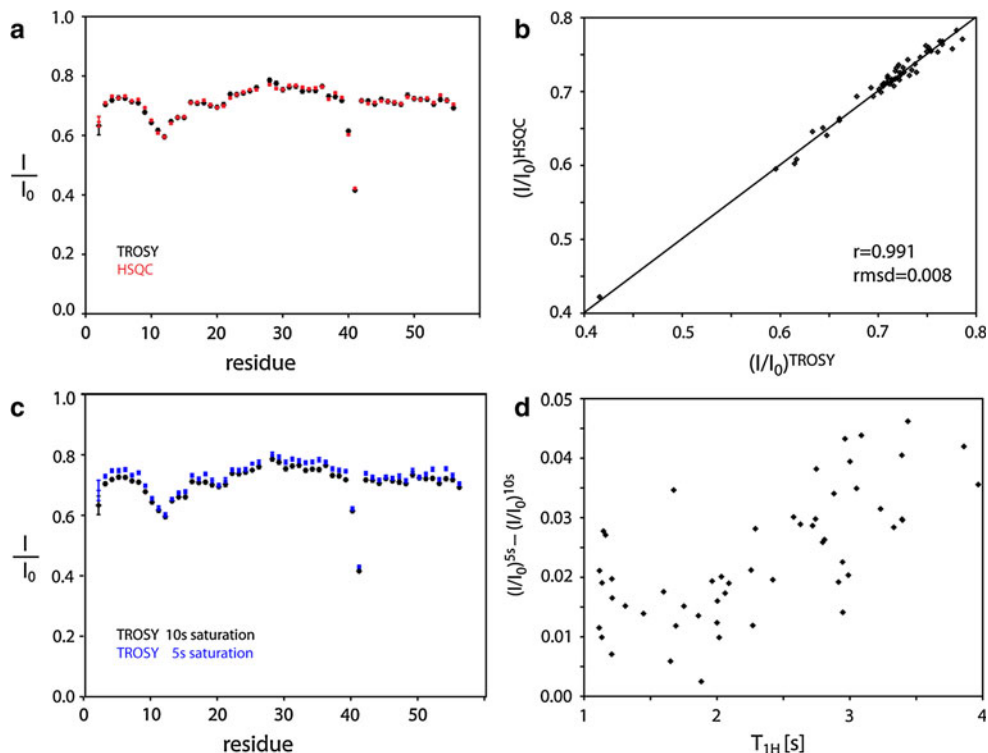
$^{15}\text{N}\{-^1\text{H}\}$ NOE measurement

Measurement of accurate $^{15}\text{N}\{-^1\text{H}\}$ NOE values by TROSY methods in perdeuterated proteins is particularly challenging for a number of reasons. First, the longitudinal

relaxation rate of isolated amide protons in the core of a deuterated protein can be an order of magnitude slower than in protonated proteins (Ulmer et al. 2004). It is important to note that even though ^1H saturation in the experiment with ^1H irradiation is very fast, full longitudinal relaxation of ^1H is required in the reference experiment, which requires an interscan delay that is long compared to the elevated $T_{1\text{H}}$ in the deuterated protein. Similarly, in both the reference and attenuated experiment, the interscan delay also needs to be long relative to the ^{15}N T_1 , which can be several seconds in larger proteins at high magnetic fields. Second, as the experiment detects the amount of ^{15}N Boltzmann magnetization after the presence or absence of ^1H saturation, it is important that in neither the saturated nor the reference experiment any antiphase terms of the type $N_z H_z$ are created. Even if only 0.1 % of ^1H magnetization inadvertently is converted into a $2N_z H_z$ term, this causes a 1 % change in the observed TROSY intensity, and a corresponding perturbation of the measured NOE. Third, as pointed out previously (Favier and Brutscher 2011), the TROSY $^{15}\text{N} \rightarrow ^1\text{H}$ readout element also functions as a $^1\text{H} \rightarrow ^{15}\text{N}$ refocused INEPT scheme (Borum and Ernst 1980), meaning that just prior to ^1H detection in the reference experiment, all Boltzmann ^1H magnetization is transferred to ^{15}N , causing a perturbation by a factor of nearly -10 from thermal equilibrium. Decay of the ^{15}N magnetization to its Boltzmann equilibrium value then would take ca $2.3 \times T_1^{15\text{N}}$ longer compared to starting from a saturated ^{15}N state, which applies in HSQC-detected experiments. In particular in the absence of ^1H saturation, i.e. the “reference experiment”, the applicable $T_1^{15\text{N}}$ value can be long due to the effect of cross-correlated relaxation (see above). However, the ^{15}N magnetization, transferred from ^1H , is easily destroyed by application of a 90° ^{15}N pulse at the end of the ^1H acquisition period. In principle, the ^{15}N magnetization can also be destroyed by application of a short duration of ^{15}N composite pulse decoupling (Zhu et al. 2000). However, the net rotation resulting from such a decoupling burst typically deviates from 90°, and complete saturation requires a decoupling duration much longer than $1/(R_1/2 + R_2/2)$.

For the NOE reference experiment, it is important that both the ^{15}N and ^1H magnetizations have returned to Boltzmann equilibrium values prior to the start of each scan. While for protonated proteins, ^1H T_1 values are usually relatively short, 1–1.5 s, for perdeuterated proteins the amide ^1H T_1 values can be longer than 10 s (Ulmer et al. 2004). Values in the small GB3 protein, studied here at room temperature, fall in the 1–4 s range (SM Fig. S2e). Indeed the discrepancy between NOEs measured using a $(5 + 1)$ -s saturation/recovery delay and a $(10 + 1)$ -s delay is more severe for residues with long $T_{1\text{H}}$ times (Fig. 5d). Faster R_1 relaxation for the downfield $^1\text{H}\{-^{15}\text{N}\}$ doublet

Fig. 5 Comparison of $^{15}\text{N}\{-^1\text{H}\}$ NOE values, I/I_0 , in GB3, measured with the pulse schemes of Fig. 1c and SM Fig. S1c. **a** $^{15}\text{N}\{-^1\text{H}\}$ NOE values measured with TROSY (black) and sensitivity-enhanced HSQC readout (red), both measured using a (10 + 1 s) saturation/recovery delay. **b** Correlation plot between $^{15}\text{N}\{-^1\text{H}\}$ NOE values measured with TROSY readout and sensitivity-enhanced HSQC readout. **c** NOE values measured with TROSY readout using a 5-s saturation/recovery delay (blue) and a 10-s delay (black). **d** The difference between NOE values measured using a (5 + 1)-s delay and a (10 + 1)-s delay versus $T_{1\text{H}}$. The non-selective ^1H $T_{1\text{H}}$ times were measured using a sensitivity-enhanced HSQC experiment (see SM Fig. S2e)



component than for the upfield component, caused by relaxation interference between the ^1H CSA and the $^1\text{H}\text{-}^{15}\text{N}$ dipolar coupling, results in buildup of antiphase H_zN_z terms, an effect that is amplified tenfold when observed through the ^{15}N TROSY intensity (see above). Although such a term is attenuated by application of a ^1H 90° purge pulse, combined with a soft pulse to return the water magnetization back to +z (Chill et al. 2006), we find this leads to small errors in the NOE, as the upfield and downfield components of the $^1\text{H}\text{-}\{^{15}\text{N}\}$ doublet rotate through slightly different trajectories. Instead, we utilize the faster relaxation of the upfield component of the $^{15}\text{N}\{-^1\text{H}\}$ doublet for TROSY readout (compare also Ferrage et al. 2008), by interchanging it with the downfield component during the gradient encoding step of the experiment (Fig. 1c). To accomplish this, a composite ^1H inversion pulse is applied simultaneously with the $180^\circ_{\phi 7}$ pulse, surrounded by two water-flip-back pulses. Note that reduction in the duration of the required interscan delay time is not dramatic, however, and the minimum delay between scans must remain long compared to the longest ^1H T_1 value, which can be very long in perdeuterated proteins (Fig. S2e).

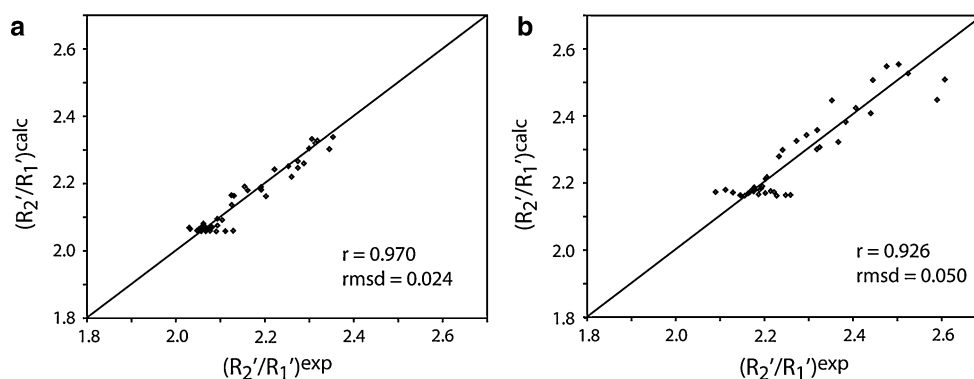
Finally, it is important that during the experiment which includes ^1H saturation, this saturation is accomplished as effective as possible, but without significantly heating the sample by the ^1H saturation pulses. Historically, 120° pulses often have been used for this purpose (Markley 1971; Kay et al. 1989). Following Ferrage et al. (2008,

2009, 2010), we use a train of 180° pulses, spaced by a multiple of $1/{}^1\text{J}_{\text{NH}}$ (22 ms) with the carrier switched to the center of the amide region, to avoid the generation of H_zN_z terms during the saturation pulse train. Indeed, small differences between this saturation scheme and saturation by 150° can be detected (data not shown) with the Ferrage scheme giving slightly improved agreement between the TROSY- and HSQC-detected experiment. When a long interscan delay is used (1 s recovery, plus 10 s on/off ^1H saturation), TROSY- and HSQC-detected experiments yield indistinguishable results, with a Pearson's correlation coefficient of 0.991 and a RMSD of 0.008 (Fig. 5a,b). When shortening the ^1H saturation to 1 + 5 s, a systematic artifactual increase by ca 0.035 is observed for the HSQC-detected experiment (Supplementary Fig. S2c) and an even larger increase by 0.076, on average, for a previous implementation of the TROSY detected experiment (compare SM Fig. S2d). Recording the spectra with the same, too short duration of ^1H saturation, but using TROSY detection and the interchange of the downfield and upfield ^{15}N TROSY components during the gradient-encoding step, reduces this artifactual increase to 0.018 but does not completely eliminate it (Fig. 5c).

Evaluation of accuracy

To assess how well the determined R_2/R_1 ratios correlate with the NH vector orientations, an axially symmetric

Fig. 6 Back-calculated versus experimental R_2'/R_1' . **a** Data measured using the pulse schemes of Fig. 1 on perdeuterated GB3. **b** Data previously measured with the original pulse schemes on protonated GB3 (Hall and Fushman 2006)



diffusion tensor has been fitted to the GB3 NMR structure (2OED) using the program ROTDIF (Walker et al. 2004). As noted earlier (Hall and Fushman 2003), an axially symmetric diffusion tensor fits the relaxation data significantly better than an isotropic one. We also find that further improvement obtained when fitting a fully anisotropic tensor is statistically not significant (data not shown). Below, we compare the fits obtained with the TROSY-detected methods for perdeuterated GB3 with the best available literature data obtained with standard HSQC-detected methods on protonated GB3 (Hall and Fushman 2006). All residues with a $^{15}\text{N}\{-^1\text{H}\}$ NOE value <0.65 were excluded from the analysis. For the fitting of the R_2'/R_1' ratio, high-frequency contributions to the spectral densities were subtracted from the relaxation rates as described in (Fushman and Cowburn 1998, 1999; Fushman et al. 1998). This removal of the $J(\omega_{\text{N}})$ and $J(\omega_{\text{H}})$ spectral density terms makes the resulting ratio R_2'/R_1' less sensitive to site-specific variations of the CSA tensor and sub-nanosecond backbone dynamics, and it then is dominated by the orientation of the NH vector relative to the diffusion tensor frame. The analysis was repeated with available literature data (Hall and Fushman 2006).

Excellent agreement between our experimental data and best-fitted R_2'/R_1' ratios (Fig. 6) support the high quality of the data, and show a level of agreement with the protein structure that is comparable to what is seen for RDC data, and even higher than previously obtained for protonated GB3 ($R_p = 0.926$).

Concluding remarks

Although conceptually straightforward, accurate measurement of ^{15}N relaxation through ^1H detection using TROSY-based detection schemes presents a number of challenges beyond those encountered in the widely used HSQC-detection based schemes. The pulse schemes introduced here have been optimized to minimize systematic errors, and make it possible to analyze reliably the

internal dynamics of larger proteins or protein complexes, where perdeuteration and TROSY detection are needed the most. The set of ^{15}N R_1 , R_2 relaxation and $^{15}\text{N}\{-^1\text{H}\}$ NOE experiments presented in this study yield results that are indistinguishable within the very small, random experimental error, from HSQC-detected experiments and is suitable for perdeuterated proteins. The high accuracy of the results also is reflected in exceptionally close agreement between orientations of the N–H vectors and the R_2'/R_1' ratios obtained from the relaxation data.

Acknowledgments We thank Dennis A Torchia and Alex Grishaev for helpful discussions and computer simulations, Frank Delaglio for assistance with the evaluation of relaxation data and Alex Maltsev for help with the expression and purification of GB3. This work was funded by the Intramural Research Program of the National Institute of Diabetes and Digestive and Kidney Diseases, National Institutes of Health (NIH) and the Intramural AIDS-Targeted Antiviral Program of the Office of the Director, NIH.

References

- Bothnerby AA, Shukla R (1988) Spin-locked states of homonuclear 2-spin systems. *J Magn Reson* 77:524–535
- Boyd J, Hommel U, Campbell ID (1990) Influence of cross-correlation between dipolar and anisotropic chemical shift relaxation mechanisms upon longitudinal relaxation rates of ^{15}N in macromolecules. *Chem Phys Lett* 175:477–482
- Burum DP, Ernst RR (1980) Net polarization transfer via a J-ordered state for signal enhancement of low-sensitivity nuclei. *J Magn Reson* 39:163–168
- Cavanagh J, Fairbrother WJ, Palmer AG, Rance M, Skelton N (2007) *Protein NMR spectroscopy: principles and practice*. Elsevier Academic Press, Burlington
- Chen K, Tjandra N (2011) Water proton spin saturation affects measured protein backbone (^{15}N) spin relaxation rates. *J Magn Reson* 213:151–157
- Chiapparini E, Pelupessy P, Ghose R, Bodenhausen G (1999) Relaxation of two-spin coherence due to cross-correlated fluctuations of dipole–dipole couplings and anisotropic shifts in NMR of N- ^{15}N , C- ^{13}C -labeled biomolecules. *J Am Chem Soc* 121:6876–6883
- Chill JH, Louis JM, Baber JL, Bax A (2006) Measurement of N- 15 relaxation in the detergent-solubilized tetrameric KcsA potassium channel. *J Biomol NMR* 36:123–136

- Delaglio F, Grzesiek S, Vuister GW, Zhu G, Pfeifer J, Bax A (1995) NMRpipe—a multidimensional spectral processing system based on unix pipes. *J Biomol NMR* 6:277–293
- Farrow NA, Muhandiram R, Singer AU, Pascal SM, Kay CM, Gish G, Shoelson SE, Pawson T, Forman-Kay JD, Kay LE (1994) Backbone dynamics of a free and a phosphopeptide-complexed Src homology 2 domain studied by ^{15}N NMR relaxation. *Biochemistry* 33:5984–6003
- Favier A, Brutscher B (2011) Recovering lost magnetization: polarization enhancement in biomolecular NMR. *J Biomol NMR* 49:9–15
- Felli IC, Desvaux H, Bodenhausen G (1998) Local mobility of N-15 labeled biomolecules characterized through cross-correlation rates: applications to paramagnetic proteins. *J Biomol NMR* 12: 509–521
- Ferrage F, Piserchio A, Cowburn D, Ghose R (2008) On the measurement of N-15- $\{^1\text{H}\}$ nuclear Overhauser effects. *J Magn Reson* 192:302–313
- Ferrage F, Cowburn D, Ghose R (2009) Accurate sampling of high-frequency motions in proteins by steady-state $(^{15}\text{N}\{-^1\text{H}\})$ nuclear Overhauser effect measurements in the presence of cross-correlated relaxation. *J Am Chem Soc* 131: 6048–+
- Ferrage F, Reichel A, Battacharya S, Cowburn D, Ghose R (2010) On the measurement of $(^{15}\text{N}\{-^1\text{H}\})$ nuclear Overhauser effects. 2. Effects of the saturation scheme and water signal suppression. *J Magn Reson* 207:294–303
- Freeman R, Kempell SP, Levitt MH (1980) Radiofrequency pulse sequences which compensate their own imperfections. *J Magn Reson* 38:453–479
- Fushman D, Cowburn D (1998) Model-independent analysis of N-15 chemical shift anisotropy from NMR relaxation data. Ubiquitin as a test example. *J Am Chem Soc* 120:7109–7110
- Fushman D, Cowburn D (1999) The effect of noncollinearity of N-15-H-1 dipolar and N-15 CSA tensors and rotational anisotropy on N-15 relaxation, CSA/dipolar cross correlation, and TROSY. *J Biomol NMR* 13:139–147
- Fushman D, Tjandra N, Cowburn D (1998) Direct measurement of N-15 chemical shift anisotropy in solution. *J Am Chem Soc* 120:10947–10952
- Fushman D, Xu R, Cowburn D (1999) Direct determination of changes of interdomain orientation on ligation: use of the orientational dependence of N-15 NMR relaxation in Abl SH(32). *Biochemistry* 38:10225–10230
- Garwood M, Ke Y (1991) Symmetrical pulses to induce arbitrary flip angles with compensation for RF inhomogeneity and resonance offsets. *J Magn Reson* 94:511–525
- Geen H, Freeman R (1991) Band-selective radiofrequency pulses. *J Magn Reson* 93:93–141
- Grzesiek S, Bax A (1993) The importance of not saturating H_2O in protein NMR. Application to sensitivity enhancement and NOE measurement. *J Am Chem Soc* 115:12593
- Hall JB, Fushman D (2003) Characterization of the overall and local dynamics of a protein with intermediate rotational anisotropy: differentiating between conformational exchange and anisotropic diffusion in the B3 domain of protein G. *J Biomol NMR* 27: 261–275
- Hall JB, Fushman D (2006) Variability of the N-15 chemical shielding tensors in the B3 domain of protein G from N-15 relaxation measurements at several fields. Implications for backbone order parameters. *J Am Chem Soc* 128:7855–7870
- Hansen DF, Kay LE (2007) Improved magnetization alignment schemes for spin-lock relaxation experiments. *J Biomol NMR* 37:245–255
- Hare BJ, Wyss DF, Osburne MS, Kern PS, Reinherz EL, Wagner G (1999) Structure, specificity and CDR mobility of a class II restricted single-chain T-cell receptor. *Nat Struct Biol* 6:574–581
- Hornak V, Abel R, Okur A, Strockbine B, Roitberg A, Simmerling C (2006) Comparison of multiple amber force fields and development of improved protein backbone parameters. *Prot Struct Funct Bioinform* 65:712–725
- Ishima R, Torchia DA (2000) Protein dynamics from NMR. *Nat Struct Biol* 7:740–743
- Kay LE (1998) Protein dynamics from NMR. *Nat Struct Biol* 5:13–517
- Kay LE, Torchia DA, Bax A (1989) Backbone dynamics of proteins as studied by ^{15}N inverse detected heteronuclear NMR spectroscopy: application to staphylococcal nuclease. *Biochemistry* 28:8972–8979
- Kay LE, Keifer P, Saarinen T (1992) Pure absorption gradient enhanced heteronuclear single quantum correlation spectroscopy with improved sensitivity. *J Am Chem Soc* 114:10663–10665
- Kern D, Zuiderweg ERP (2003) The role of dynamics in allosteric regulation. *Curr Opin Struct Biol* 13:748–757
- Kobzar K, Skinner TE, Khaneja N, Glaser SJ, Luy B (2008) Exploring the limits of broadband excitation and inversion: II. Rf-power optimized pulses. *J Magn Reson* 194:58–66
- Korzhev DM, Skrynnikov NR, Millet O, Torchia DA, Kay LE (2002) An NMR experiment for the accurate measurement of heteronuclear spin-lock relaxation rates. *J Am Chem Soc* 124: 10743–10753
- Lee AL, Wand AJ (2001) Microscopic origins of entropy, heat capacity and the glass transition in proteins. *Nature* 411:501–504
- Lee AL, Kinnear SA, Wand AJ (2000) Redistribution and loss of side chain entropy upon formation of a calmodulin-peptide complex. *Nat Struct Biol* 7:72–77
- Li D-W, Brueschweiler R (2009) A dictionary for protein side-chain entropies from NMR order parameters. *J Am Chem Soc* 131: 7226–7227
- Markley JL, Horsley WJ, Klein MP (1971) Spin-lattice relaxation measurements in slowly relaxing complex spectra. *J Chem Phys* 55:3604–3605
- Massi F, Johnson E, Wang CY, Rance M, Palmer AG (2004) NMR R-1 rho rotating-frame relaxation with weak radio frequency fields. *J Am Chem Soc* 126:2247–2256
- Millet O, Muhandiram DR, Skrynnikov NR, Kay LE (2002) Deuterium spin probes of side-chain dynamics in proteins. 1. Measurement of five relaxation rates per deuteron in C-13-labeled and fractionally H-2-enriched proteins in solution. *J Am Chem Soc* 124:6439–6448
- Mitschang L, Keeler J, Davis AL, Oschkinat H (1992) Removal of zero-quantum interference in NOESY spectra of proteins by utilizing the natural inhomogeneity of the radiofrequency field. *J Biomol NMR* 2:545–556
- Mittag T, Kay LE, Forman-Kay JD (2010) Protein dynamics and conformational disorder in molecular recognition. *J Mol Recognit* 23:105–116
- Mittermaier A, Kay LE (2006) Review—new tools provide new insights in NMR studies of protein dynamics. *Science* 312: 224–228
- Muhandiram DR, Yamaaki T, Sykes BD, Kay LE (1995) Measurement of ^2H T1 and T1 ρ relaxation times in uniformly ^{13}C -labeled and fractionally ^2H -labeled proteins in solution. *J Am Chem Soc* 117:11536–11544
- Mulder FAA, de Graaf RA, Kaptein R, Boelens R (1998) An off-resonance rotating frame relaxation experiment for the investigation of macromolecular dynamics using adiabatic rotations. *J Magn Reson* 131:351–357
- Nadaud PS, Helmuss JJ, Jaroniec CP (2007) ^{13}C and ^{15}N chemical shift assignments and secondary structure of the B3 immunoglobulin-binding domain of streptococcal protein G by magic-angle spinning solid-state NMR spectroscopy. *Biomol NMR Assign* 1:117–120

- Namanja AT, Wang XJ, Xu B, Mercedes-Camacho AY, Wilson KA, Etkorn FA, Peng JW (2011) Stereospecific gating of functional motions in Pin1. *Proc Natl Acad Sci USA* 108:12289–12294
- Nietlispach D (2005) Suppression of anti-TROSY lines in a sensitivity enhanced gradient selection TROSY scheme. *J Biomol NMR* 31:161–166
- Nirmala NR, Wagner G (1988) Measurement Of C-13 relaxation-times in proteins by two-dimensional heteronuclear H1-C-13 correlation spectroscopy. *J Am Chem Soc* 110:7557–7558
- Palmer AG (2004) NMR characterization of the dynamics of biomacromolecules. *Chem Rev (Washington, DC, US)* 104:3623–3640
- Pelupessy P, Chiarparin E, Ghose R, Bodenhausen G (1999) Simultaneous determination of Psi and Phi angles in proteins from measurements of cross-correlated relaxation effects. *J Biomol NMR* 14:277–280
- Peng JW, Wagner G (1992) Mapping of spectral density functions using heteronuclear NMR relaxation measurements. *J Magn Reson* 98:308–332
- Peng JW, Thanabal V, Wagner G (1991) 2d heteronuclear NMR measurements of spin-lattice relaxation-times in the rotating frame of X nuclei in heteronuclear HX spin systems. *J Magn Reson* 94:82–100
- Pervushin K, Riek R, Wider G, Wuthrich K (1997) Attenuated T-2 relaxation by mutual cancellation of dipole–dipole coupling and chemical shift anisotropy indicates an avenue to NMR structures of very large biological macromolecules in solution. *Proc Natl Acad Sci USA* 94:12366–12371
- Pervushin KV, Wider G, Wuthrich K (1998) Single transition-to-single transition polarization transfer (ST2-PT) in [N15, H1]-TROSY. *J Biomol NMR* 12:345–348
- Piotto M, Saudek V, Sklenár V (1992) Gradient-tailored excitation for single-quantum NMR spectroscopy of aqueous solutions. *J Biomol NMR* 2:661–665
- Popovych N, Sun S, Ebright RH, Kalodimos CG (2006) Dynamically driven protein allostery. *Nat Struct Mol Biol* 13:831–838
- Price DJ, Brooks CL (2002) Modern protein force fields behave comparably in molecular dynamics simulations. *J Comput Chem* 23:1045–1057
- Reif B, Hennig M, Griesinger C (1997) Direct measurement of angles between bond vectors in high-resolution NMR. *Science* 276:1230–1233
- Rinenthal J, Buck J, Ferner J, Wacker A, Fuertig B, Schwalbe H (2011) Mapping the landscape of RNA dynamics with NMR spectroscopy. *Acc Chem Res* 44:1292–1301
- Showalter SA, Bruschweiler R (2007) Validation of molecular dynamics simulations of biomolecules using NMR spin relaxation as benchmarks: application to the AMBER99SB force field. *J Chem Theory Comput* 3:961–975
- Sklenar V, Torchia D, Bax A (1987) Measurement of C-13 longitudinal relaxation using H-1 detection. *J Magn Reson* 73:375–379
- Smith MA, Hu H, Shaka AJ (2001) Improved broadband inversion performance for NMR in liquids. *J Magn Reson* 151:269–283
- Stocker U, van Gunsteren WF (2000) Molecular dynamics simulation of hen egg white lysozyme: a test of the GROMOS96 force field against nuclear magnetic resonance data. *Prot Struct Funct Genet* 40:145–153
- Stone MJ (2001) NMR relaxation studies of the role of conformational entropy in protein stability and ligand binding. *Acc Chem Res* 34:379–388
- Tjandra N, Feller SE, Pastor RW, Bax A (1995) Rotational diffusion anisotropy of human ubiquitin from N-15 NMR relaxation. *J Am Chem Soc* 117:12562–12566
- Tjandra N, Szabo A, Bax A (1996) Protein backbone dynamics and N-15 chemical shift anisotropy from quantitative measurement of relaxation interference effects. *J Am Chem Soc* 118:6986–6991
- Ulmer TS, Campbell ID, Boyd J (2004) Amide proton relaxation measurements employing a highly deuterated protein. *J Magn Reson* 166:190–201
- Varadan R, Assfalg M, Haririnia A, Raasi S, Pickart C, Fushman D (2004) Solution conformation of Lys(63)-linked di-ubiquitin chain provides clues to functional diversity of polyubiquitin signaling. *J Biol Chem* 279:7055–7063
- Walker O, Varadan R, Fushman D (2004) Efficient and accurate determination of the overall rotational diffusion tensor of a molecule from N-15 relaxation data using computer program ROTDIF. *J Magn Reson* 168:336–345
- Wang AC, Bax A (1993) Minimizing the effects of radiofrequency heating in multidimensional NMR experiments. *J Biomol NMR* 3:715–720
- Yang DW, Mok YK, FormanKay JD, Farrow NA, Kay LE (1997) Contributions to protein entropy and heat capacity from bond vector motions measured by NMR spin relaxation. *J Mol Biol* 272:790–804
- Yang DW, Mittermaier A, Mok YK, Kay LE (1998) A study of protein side-chain dynamics from new H-2 auto-correlation and C-13 cross-correlation NMR experiments: application to the N-terminal SH3 domain from drk. *J Mol Biol* 276:939–954
- Zhu G, Xia YL, Nicholson LK, Sze KH (2000) Protein dynamics measurements by TROSY-based NMR experiments. *J Magn Reson* 143:423–426
- Zidek L, Novotny MV, Stone MJ (1999) Increased protein backbone conformational entropy upon hydrophobic ligand binding. *Nat Struct Biol* 6:1118–1121